



1 Contribution of Rock Glacier Discharge to Late-Summer and 2 Fall Streamflow in the Uinta Mountains, Utah, USA

3
4 Jeffrey S. Munroe¹, Alexander L. Handwerger^{2,3}

5 ¹ Geology Department, Middlebury College, Middlebury, 05753, USA

6 ² Joint Institute for Regional Earth System Science and Engineering, University of California, Los Angeles, 90095,
7 USA

8 ³ Jet Propulsion Laboratory, California Institute of Technology, Pasadena, 91109, USA

9 *Correspondence to:* Jeffrey S. Munroe (jmunroe@middlebury.edu)

10

11 **Abstract.** Water draining from rock glaciers in the Uinta Mountains of Utah (USA) was analyzed and compared
12 with samples of ground water and water from the master stream in a representative 5000-ha drainage. Rock glacier
13 water resembles snowmelt in the early summer, but transitions to higher values of *d-excess* and greatly elevated Ca
14 and Mg content as the melt season progresses. This pattern is consistent with models describing a transition from
15 snowmelt, to melting of seasonal ice, to melting of perennial ice in the rock glacier interior in late summer and fall.
16 Water derived from this internal ice appears to have been the source of ~25% of the streamflow in this study area
17 during September of 2021. This result emphasizes the significant role that rock glaciers can play in the hydrology of
18 high-elevation watersheds, particularly in summers following a winter with below average snowpack.

19

20 **Keywords:** Rock glacier; hydrology; permafrost; stable isotopes; climate change

21

22 1 Introduction

23 Contemporary climate change is responsible for an array of dramatic effects in high mountain environments (Adler
24 et al., 2019; Chakraborty, 2021). Average temperatures of air (Bonfils et al., 2008; Minder et al., 2018) and
25 permafrost (Biskaborn et al., 2019) are rising, glaciers are retreating (Sakai and Fujita, 2017; Sommer et al., 2020),
26 the ranges of plants (Alexander et al., 2018; Albrich et al., 2020) and animals (Millar and Westfall, 2010; Rödder et
27 al., 2021) are shifting, and ecosystem services (Egan and Price, 2017; Palomo, 2017) and the societies that depend
28 on them (McDowell et al., 2019; Xenarios et al., 2019) are in a phase of readjustment. Documenting and
29 understanding these changes is of crucial importance in mitigating natural hazards (Stoffel and Corona, 2018; Thaler
30 et al., 2018), anticipating future scarcity of water resources (Beniston et al., 2018; Rowan et al., 2018), designing
31 appropriate conservation strategies (Catalan et al., 2017), and planning for a future in which mountain environments
32 look and function differently than they have for the past century (Huss et al., 2017).



33 A component of mountain landscapes with strong potential to document past and present environmental
34 changes, and a notable vulnerability to climatic perturbations, are features known as rock glaciers. Typically present
35 in cold environments that are too dry for the formation of ice glaciers, rock glaciers are mixtures of rock debris and
36 perennial ice that move downslope through a combination of creep and basal shear (Wahrhaftig and Cox, 1959;
37 Giardino et al., 1987; Giardino and Vitek, 1988). Given their genesis, their composition, and their behavior, rock
38 glaciers exist at the intersection of climate, the cryosphere, and hydrology.

39 Traditionally, rock glacier research focused on the distribution and paleoclimatic significance of these
40 features (Konrad et al., 1999; Johnson et al., 2021). Modern updates to these investigations are applying high
41 precision GPS (Buchli et al., 2018), photogrammetry (Kenner et al., 2018), surface-exposure dating (Lehmann et al.,
42 2022), and remote sensing to monitor rock glacier movement (Strozzi et al., 2020), offering an unprecedented
43 understanding of the relationship between rock glacier behavior and climate change. Studies have also sought to
44 explore the role of rock glaciers as refugia for cold-adapted organisms in the face of warming temperatures (Millar
45 et al., 2015; Brighenti et al., 2021).

46 An additional line of inquiry with critical importance in regions characterized by water scarcity is the
47 contribution of rock glaciers to high mountain hydrology (Rangecroft et al., 2015; Jones et al., 2019). The
48 interconnected pore space within the typically coarse debris comprising a rock glacier allows these features to serve
49 as aquifers, storing and releasing water over a variety of timescales (Geiger et al., 2014; Harrington et al., 2018;
50 Wagner et al., 2020; Halla et al., 2021). Moreover, perennial ice within the interior of an active rock glacier is a
51 reservoir of longer-term storage that is nonetheless vulnerable to being lost from the system through melting in
52 excess of new ice formation. Studies have investigated the ice content of rock glaciers using geophysical methods
53 like ground penetrating radar and invasive approaches like drilling (Krainer and Mostler, 2002; Krainer et al., 2015;
54 Petersen et al., 2020; Wagner et al., 2021). Extrapolation from these investigations, and incorporation of empirical
55 transfer functions, has supported estimates of rock glacier water storage for some areas (Azócar and Brenning, 2010;
56 Rangecroft et al., 2015; Janke et al., 2017; Jones et al., 2018). Nonetheless, uncertainty remains about how much ice
57 is stored within rock glaciers, the vulnerability of this ice to climate warming, and how much ice may already be
58 melting and contributing to base flow, particularly in late summer after the melting of seasonal snow has ceased.

59 Here we investigate the water draining from representative rock glaciers in the Uinta Mountains in
60 northeastern Utah, a mountain range in which rock glaciers have been inventoried (Munroe, 2018) and monitored
61 (Brencher et al., 2021) in previous work. Automated samplers were used to collect time series of water discharging
62 from two rock glaciers, a non-rock glacier spring, and along the master stream. All samples were analyzed for
63 cation chemistry and stable isotopes to test two related hypotheses: 1) that the rock glacier springs would exhibit
64 properties distinct from the other water sources and consistent with the melting of internal ice in late summer; and 2)
65 that late summer streamflow along the master stream would contain a non-trivial amount of rock glacier-sourced
66 water.

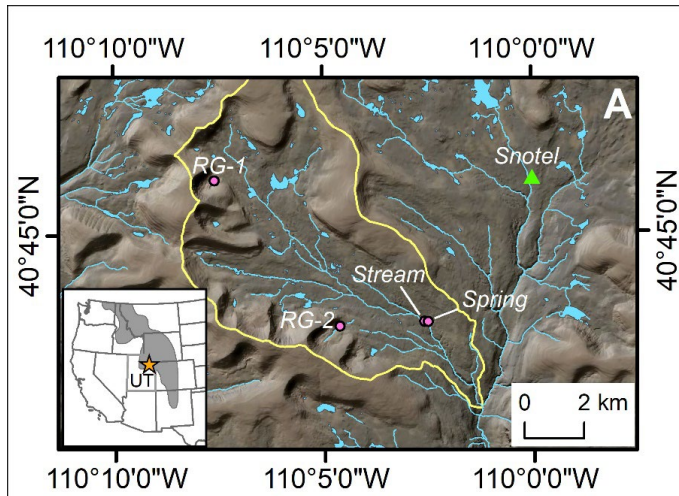
67



68 2 Study Area

69 The study area for this project is in the upper West Fork Whiterocks River watershed in the southeastern sector of
70 the Uinta Mountains (Figure 1). The watershed has an area of ~5000 ha above the lowest sampling site, and
71 elevations range from 2960 to over 3700 m. The Uinta Mountains (hereafter, the “Uintas”) are a substantial
72 component of the Rocky Mountain system located in northeastern Utah in the western United States. The Uintas are
73 the highest mountains in this region, reaching elevations in excess of 4 km. Geologically, the bedrock of the Uintas
74 is a thick sequence of Precambrian siliciclastic rocks that was uplifted during the Laramide orogeny beginning in the
75 early Paleogene (Sears et al., 1982; Hansen, 1986; Dehler et al., 2007). Pleistocene valley glaciers eroded deep
76 cirques and glacial canyons, and deposited massive lateral and end moraine systems (Atwood, 1909; Munroe and
77 Laabs, 2009). No glaciers remain in the Uintas today, however the climate at higher elevations, where mean annual
78 temperatures are $<0^{\circ}\text{C}$ (Munroe, 2006), supports patterned ground, talus, and abundant rock glaciers. Previous
79 work using optical imagery (Munroe, 2018) and satellite-based radar interferometry (Brencher et al., 2021)
80 identified more than 200 active rock glaciers in the Uintas, and many more rock glaciers that are no longer moving.

81



82

83 **Figure 1:** Location Map of the study area. Inset shows location of the Uinta Mountains (orange star) within the state
84 of Utah (UT). Gray shaded polygon represents the Rocky Mountains. Map presents the upper Whiterocks River
85 watershed (yellow boundary), the locations of the RG-1, RG-2, Stream, and Spring water samplers (pink circles),
86 and the Chepeta SNOTEL site (green triangle).

87

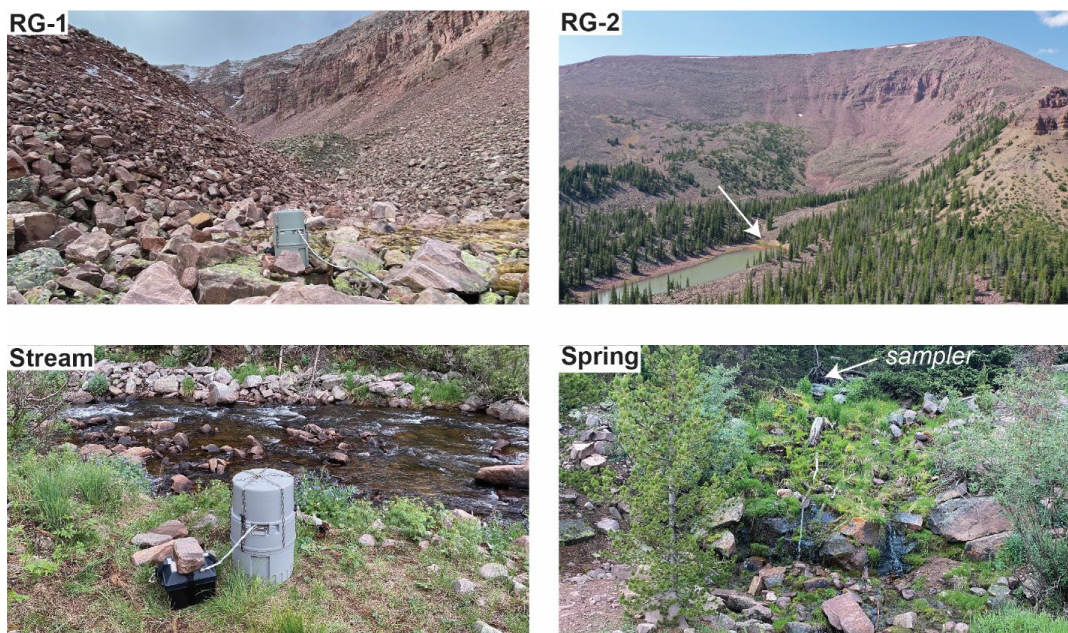
88 3 Methods

89 This project centered on the collection of time series of water samples using automated samplers outfitted with a
90 carousel of 24 bottles. The samples were deployed with a solar powered battery system, allowing them to run



91 throughout the summer with no maintenance. To reduce the possibility of isotopic fractionation related to
92 evaporation, sample bottles were modified following published methodology (von Freyberg et al., 2020). In each
93 location, the samplers were deployed in a position higher than their water intake to facilitate free draining of the
94 intake hose between samples. The weighted strainer on the end of the water intake line was wrapped in 100- μ m
95 nylon mesh to prevent coarse material from clogging the sampler pump. Each sampler was programmed to collect a
96 45-mL sample twice each day, at midnight and noon. For three days these samples (six samples total) were
97 composited in a single bottle, thus the 24 bottles in each sampler represented a maximum deployment duration of 72
98 days.

99 Two samplers were deployed at springs discharging from the base of rock glaciers that were the focus of
100 previous investigations (Munroe, 2018). These features, “RG-1” and “RG-2”, are typical of cirque floor, tongue-
101 shaped rock glaciers in the Uinta Mountains (Figures 1 and 2).



102

103 **Figure 2:** Pictures of water samplers at RG-1, RG-2, the Stream, and the Spring sites.

104

105 Each is approximately 600 m long, 100 m wide, and has steep frontal and side slopes standing up to 20 m tall. Fresh
106 exposures on these slopes reveal that the rock glaciers consist of several meters of coarse, openwork boulders
107 overlying a diamicton with a sand matrix. Internal ice is not exposed in either rock glacier, however data loggers
108 reveal that the springs maintain a temperature of 0 °C throughout the summer, and rock glacier surface temperatures
109 equilibrate at -5 °C or colder beneath winter snow cover (Munroe, 2018). Satellite InSAR (interferometric synthetic
110 aperture radar) analysis indicates that these features move slowly during the winter and accelerate during the



111 summer to velocities of ~10 cm/yr (Brencher et al., 2021). Collectively these observations suggest the presence of
112 ice within the rock glacier interior. The spring sampled at RG-1 has a typical summer discharge of 15 L/min. The
113 discharge at RG-2 was not measured directly, but a water-level logger records diurnal fluctuations of 0.2 (early
114 summer) to 0.02 m (late summer) of the lake into which the spring flows. Given the surface area of the lake (12,000
115 m²), these daily variations suggest a discharge on the order of 10² to 10³ L/min.

116 Two other water samplers were deployed at non-rock glacier locations. The “Spring” sampler collected
117 groundwater discharging from a typical spring unrelated to a rock glacier, and the “Stream” water sampler was
118 positioned along the main channel of the West Fork Whiterocks River, the master stream in this drainage (Figure 1).
119 These samplers were configured in an identical manner to those deployed at the rock glacier springs.

120 To constrain the properties of precipitation in the study area, grab samples of snow were collected on the
121 surfaces of RG-1 and RG-2 when the water samplers were deployed. Water draining from a melting snowbank on
122 RG-2 was also collected. Rain was collected during the deployment period at the RG-2 and the Spring locations
123 using samplers of a design intended to eliminate evaporation-related fractionation of isotope values (Gröning et al.,
124 2012).

125 All samplers were installed at the beginning of July, 2021 (Table 1). At the Stream, Spring, and RG-2
126 samplers a subsample was taken from the first bottle about a week later, with the remainder left inside the sampler.
127 This procedure provided a check on the potential role of evaporation fractionating the water samples as they waited
128 inside the sampler. All bottles were emptied at the beginning of September, and the samplers were relaunched to
129 run until mid-October, when they were emptied again and deactivated for the winter. The two precipitation
130 samplers were emptied when the water samplers were serviced. All samples for stable isotope analysis were filtered
131 in the field to 0.2 μm and stored in 7-ml glass vials with Teflon-lined caps. Samples for ICP-MS analysis were
132 stored in 15-ml centrifuge tubes. These samples were vacuum filtered with Whatman Number 1 paper in the lab and
133 acidified to pH 2 with trace-element grade HNO₃. In a preliminary phase of this project, daily samples were also
134 collected at the RG-2 spring in the fall of 2020.

Table 1. Locations, Dates, and Durations of Water Sampler Deployments

Sampler	Latitude	Longitude	Elevation (m)	Deployed	Emptied	Emptied	Duration (Days)
RG-1	40.766906	-110.127608	3408	7/2/2021	9/5/2021	10/7/2021	97
RG-2	40.721883	-110.076875	3197	7/1/2021	9/2/2021	10/6/2021	97
Spring	40.723016	-110.042131	2977	7/3/2021	9/2/2021	10/6/2021	95
Stream	40.722979	-110.043123	2965	7/3/2021	9/6/2021	10/6/2021	95

135

136 Stable isotope measurements were made with a Los Gatos 45-EP Triple Liquid Water Isotope Analyzer at
137 Middlebury College. Samples were run against a bracketing set of 5 standards and calibrated with a cubic spline
138 function. Each sample was analyzed 10 times, with the first 2 injections discarded to minimize cross-over.



139 Standards were run as unknowns after every five samples as an internal check on the results. Results were
140 compared with the Global Meteoric Water Line-GMWL (Craig, 1961) as well as a Local Meteoric Water Line
141 (LMWL) estimated from OIPC, the Online Isotopes in Precipitation Calculator (Bowen and Wilkinson, 2002;
142 Bowen and Revenaugh, 2003). Values of *d-excess* were calculated as $d\text{-excess} = \delta D - (8 * \delta^{18}O)$ (Dansgaard, 1964).

143 Hydrochemical characterizations were made with a Thermo iCap ICP-MS at Middlebury College. Samples
144 were run against a set of standards derived from NIST Standard Reference Material 1643f “Trace Elements in
145 Water”. An in-house standard was used to determine the abundance of Si and Ti, which are not present in 1643f.
146 The NIST standard and the in-house standards were run after every 10 unknowns and a linear correction was applied
147 to compensate for instrument drift. Interpretation focused on elements that consistently exhibited concentrations >1
148 ppb.

149

150 4 Results

151 A total of 141 water samples was analyzed, consisting of 134 samples from the four time-series (including the 3
152 duplicates), 4 samples of rain, 2 samples of snow, and 1 sample of snow melt. The time-series are essentially
153 complete with no gaps between early July and mid-October. The lone interruption is one bottle from the Stream
154 sampler, representing 18-20 July, that was empty, apparently because the water level in the river briefly dropped
155 below the position of the intake hose.

156 Overall values of δD in the time-series range from -118.94 to -83.71‰. Values of $\delta^{18}O$ range from -16.36
157 to -12.24‰, and $\delta^{17}O$ from -9.13 to -6.39‰ (Table 2). The mean of δD is lowest in the Spring samples (-113.44‰)
158 and highest at RG-1 (-91.24‰). The same pattern holds for mean values of $\delta^{18}O$ and $\delta^{17}O$ (Table 2). Values of *d-*
159 *excess* are highest at the RG sites, and lowest (~10‰) in the Stream (Table 2). Values of δD and $\delta^{18}O$ for the
160 subsamples from the first bottle in the Stream, Spring, and RG-2 samplers are quite similar to the remainder that was
161 left inside the collector during the summer (Figure 3).

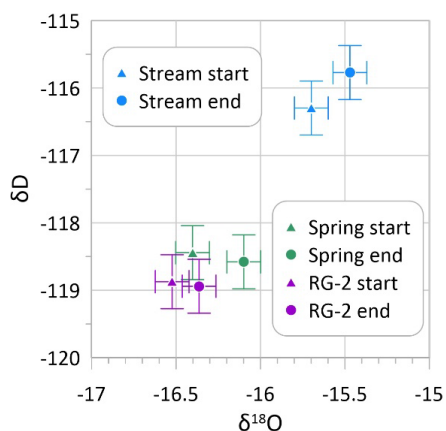


Figure 3: Comparison of isotope values measured for samples from RG-2, the Stream, and the Spring samplers. Subsamples were removed from the first sample in early July and the remainder of the water was left inside the collector until early September. Analysis of the sample pairs confirms that potential evaporation-related fractionation was minimal.

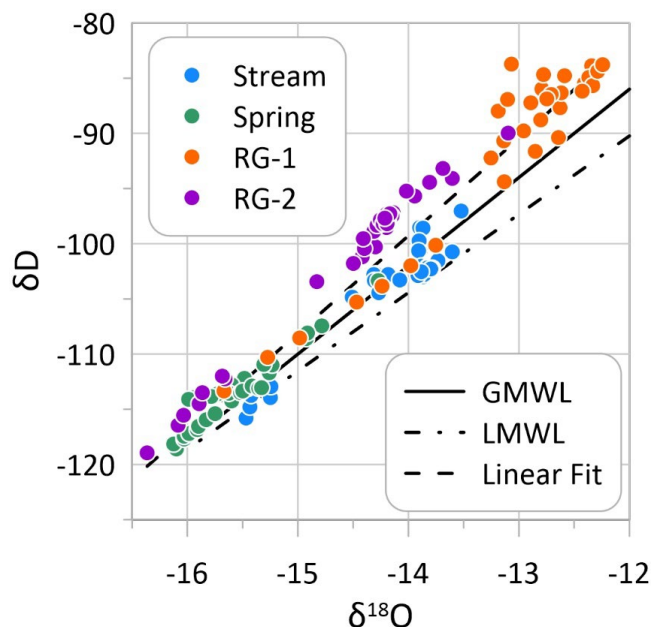
172



	$\delta^2\text{H}$ (‰)	$\delta^{18}\text{O}$ (‰)	$\delta^{17}\text{O}$ (‰)	d-Excess (‰)
Stream (n=31)				
Mean	-103.86	-14.17	-7.38	9.52
Median	-102.55	-13.90	-7.40	9.02
Standard Deviation	4.92	0.57	0.31	1.52
Minimum	-115.77	-15.47	-8.06	7.97
Maximum	-97.05	-13.52	-6.78	12.62
Spring (n=33)				
Mean	-113.44	-15.57	-8.80	11.16
Median	-113.59	-15.60	-8.84	10.79
Standard Deviation	3.25	0.42	0.20	1.03
Minimum	-118.58	-16.12	-9.13	9.57
Maximum	-103.35	-14.28	-8.30	13.80
RG-1 (n=33)				
Mean	-91.24	-13.13	-6.94	13.83
Median	-87.22	-12.80	-6.62	13.87
Standard Deviation	8.52	0.88	0.60	2.59
Minimum	-113.35	-15.67	-8.48	9.80
Maximum	-83.71	-12.24	-6.39	20.82
RG-2 (n=34)				
Mean	-101.32	-14.53	-7.52	14.93
Median	-98.27	-14.24	-7.19	15.50
Standard Deviation	7.46	0.79	0.58	1.32
Minimum	-118.94	-16.36	-8.76	11.97
Maximum	-89.99	-13.10	-6.92	16.91

173

174 Values of δD and $\delta^{18}\text{O}$ are linearly and significantly ($p < 0.001$) related with a slope of 8.8 and a Y-intercept of
 175 24.4‰ (Figure 4). Lower values of $\delta^{18}\text{O}$ plot closer to the GMWL; higher values of $\delta^{18}\text{O}$ plot increasingly above
 176 the GMWL. Plotting the data from the individual samplers separately, with color coding by month, reveals
 177 additional details (Figure 5). Values for the Stream and Spring samplers plot along the GMWL through the summer.
 178 For the Stream, the lowest values are from July with higher values in late summer and fall. For the Spring, the
 179 lowest values are again July, with the highest values in August; September and October values fall in between
 180 (Figure 5). On the other hand, for the two rock glaciers, July values are again lower and closer to the GMWL, but
 181 values from late summer and the fall plot notably above the GMWL with *d-excess* up to 20%. At RG-2, a similar
 182 pattern was noted in daily samples collected during September, 2020 (Figure 5).



183

184 **Figure 4:** Dual isotope plot of $\delta^{18}\text{O}$ and δD for the samples collected at RG-1, RG-2, the Stream, and the Spring.
185 The Global Meteoric Water Line (GMWL), a local meteoric water line (LMWL) determined from the Online
186 Isotopes in Precipitation Calculator (Bowen and Wilkinson, 2002; Bowen and Revenaugh, 2003), and a linear fit to
187 the data are presented for reference.

188

189 Plotting the data from the different samplers as time-series reveals patterns in the evolution of isotope
190 values during the sampling period (Figure 6). Given the strong correspondence between values of δD and $\delta^{18}\text{O}$,
191 only $\delta^{18}\text{O}$ is presented for clarity. Values are low at the start of the sampling period (early July), and generally rise
192 in all records through the summer and early fall (Figure 6A). The Spring and RG-2 both start below -16‰; the
193 Stream and RG-1 start slightly higher, near -15.5‰. All of the records exhibit transient spikes to less negative
194 values that occur quickly and taper gradually back to background levels (Figure 6A). These spikes align with pulses
195 of precipitation recorded at the Chepeta SNOTEL (snowpack telemetry) site <10 km to the north, and at a similar
196 elevation (Figure 1). Thus, it is likely that they represent rainstorms that delivered water less depleted in $\delta^{18}\text{O}$
197 relative to SMOW, a response reported in other studies (Krainer and Mostler, 2002). After these pulses are removed
198 from the data to highlight the background trends at each of the sites (Figure 6B), the record from the Spring is seen
199 to be the most stable, with nearly all values between -16 and -16.5‰. The water at RG-2, which started off similar
200 to the Spring, rises steadily to a maximum of -14‰ in early October. The Stream rises from -15.5‰ to -14‰ by the
201 third week of August, and stabilizes through the end of the record. Finally, RG-1, which also starts at -15.5‰, rises
202 rapidly in the first half of July, then more gradually until early September, when it peaks at -12.5‰ before dropping
203 to -13‰.

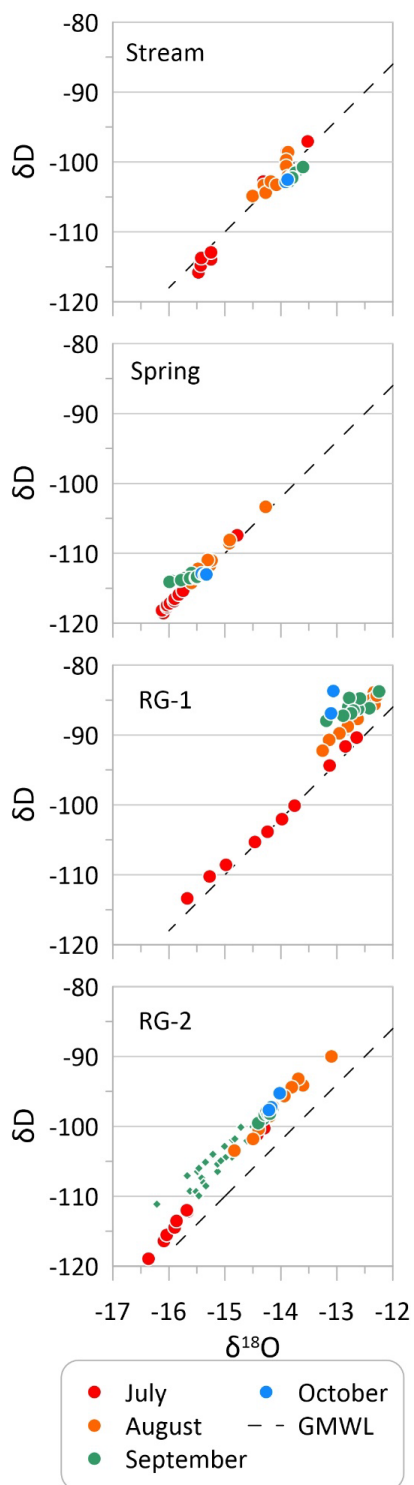
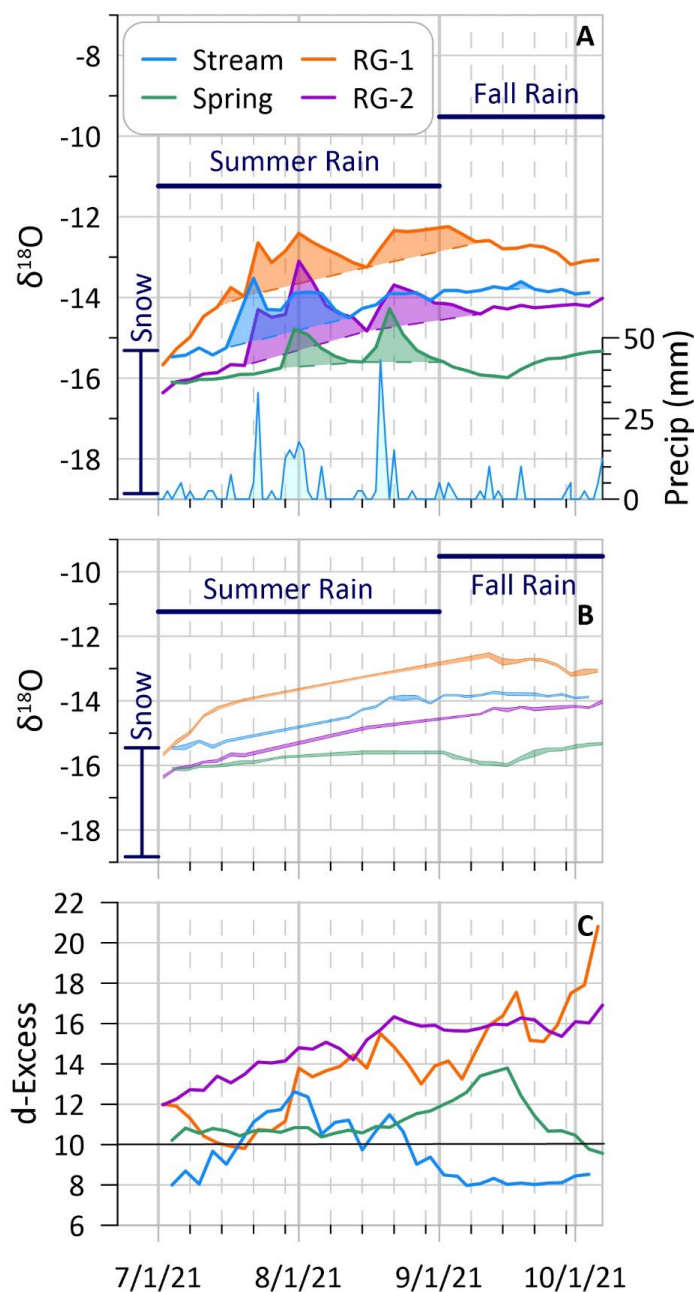


Figure 5: Dual isotope plots for the four individual time series. Color-coding represents the month of sample collection. The tendency for samples at the Stream and Spring to remain on the waterline while samples from the rock glaciers deviate to higher values of *d-excess* in late summer and fall is clearly evident. Green diamonds for RG-2 present reconnaissance data from September, 2020.



232

233 **Figure 6:** Time series from the four sampling sites. (A) Values of $\delta^{18}\text{O}$ presented along with average values for
 234 snow and rain, and daily precipitation recorded at the Chepeta SNOTEL site (Figure 1). (B) Same as Panel B with
 235 transient spikes in $\delta^{18}\text{O}$ due to precipitation events removed. (C) Times series of *d-excess*. The reference value of
 236 10‰ is highlighted.



237 Values of *d-excess* in the time-series exhibit varying patterns (Figure 6C). Values from the Stream initially rise,
238 then fall through August and stabilize at 8‰ in the fall. The Spring samples are initially stable between 10 and
239 11‰, then rise in early September to a high of 14‰, before falling back to 10‰. The two rock glaciers sites, in
240 contrast, rise steadily from near 10‰, to $\geq 17\%$ in early October (Figure 6C).

241 Context for the isotope values from the water samplers is provided by the precipitation samples collected at
242 the Spring and RG-2 sites, and grab samples of snow from RG-1 and RG-2 (Figure 6). Values of $\delta^{18}\text{O}$ in snow are
243 low, averaging -17‰. In contrast, bulk precipitation falling in July and August at the Spring and RG-2 averages -
244 11.2‰, and fall precipitation averages -9.5‰. Values of *d-excess* in snow samples are $\sim 10\%$, whereas values in
245 rain samples are 13 to 21‰.

246 Hydrochemical analysis with ICP-MS reveals 12 elements that are consistently detectable in these samples:
247 Ba, Ca, Fe, K, Mg, Mn, Na, Ni, Rb, Si, Sr, and Ti. Ca and Si are generally the most abundant cations, with mean
248 abundance ~ 1500 to 2000 ppb, followed by K, Na and K with abundances averaging 500-800 ppb. Fe and Ba are
249 generally present at abundances around 100 ppb; other elements are present at lower concentrations (Table 3).
250 Principle component analysis of these elemental concentrations, conducted with a varimax rotation, places five
251 elements (Ba, Ca, Na, Mg, Ni) on the first component (PC-1), with Ti, Rb, Si, K, Sr, and Mn on the second (PC-
252 2). Together these two components explain 78% of the variance. Highest values of PC-1 are found in the Spring
253 samples, followed by the Stream and the two rock glaciers. In contrast, PC-2 is highest at the rock glacier sites and
254 lower in the Stream and Spring. Plotting of PC-1 vs. PC-2 reveals a nearly complete separation between the rock
255 glacier water and samples from the Stream and Spring (Figure 7). When considered as time-series, values of both
256 components are generally stable at the Stream and Spring, but rise consistently through the summer and fall at RG-1
257 and RG-2 (Figure 8).

258 The same 12 cations were generally detectable in the precipitation samples, with the exception of Fe, which
259 was typically below the detection limit. Values of Na, K, Mn, Rb, Fe, Ni, and Sr were higher in snow samples
260 relative to rain, with particularly high values of Na and K in the July snow sample from the RG-2 site (Figure 9). In
261 contrast, Ca, Ti, Ba, Mg, and Si were more abundant in rain samples. All elements were less abundant in rain than
262 in the time-series.

263

264 **5 Discussion**

265 **5.1 Isotopes and Hydrochemistry**

266 The automated samplers utilized in this project were successful at collecting essentially uninterrupted sequences of
267 water throughout their deployment. Modification of the samplers effectively reduced evaporation-related
268 fractionation that could have skewed the results over the long duration deployments. As seen in Figure 3, analysis
269 of the subsample from the first sample bottle that was removed in early July yielded similar results to the water that
270 remained inside the sampler until September. Values of δD and $\delta^{18}\text{O}$ overlap within error for RG-2 and are very



Table 3: Summary Hydrochemistry

	Na (ppb)	K (ppb)	Ca (ppb)	Ti (ppb)	Mn (ppb)	Rb (ppb)	Ba (ppb)	Mg (ppb)	Si (ppb)	Fe (ppb)	Ni (ppb)	Sr (ppb)
Stream (n=31)												
Mean	848.2	465.8	1636.9	3.2	3.9	0.4	64.6	496.0	1053.2	66.9	0.8	9.0
Median	790.0	347.3	1635.9	3.2	2.4	0.3	61.6	499.7	1056.7	49.3	0.6	9.0
Standard Deviation	199.6	393.4	77.9	0.3	4.7	0.1	8.9	17.2	79.9	80.0	0.4	0.9
Minimum	605.4	262.6	1471.5	2.5	0.7	0.2	56.2	451.5	866.0	0.0	0.2	7.7
Maximum	1325.4	2264.8	1836.5	4.2	23.2	0.9	92.3	528.9	1176.2	410.1	1.6	11.2
Spring (n=33)												
Mean	1075.5	499.9	1997.5	4.4	3.3	0.3	115.6	599.0	2034.7	34.7	0.7	11.0
Median	1104.8	513.1	1860.8	3.9	3.2	0.3	104.2	579.6	2048.8	20.1	0.5	10.8
Standard Deviation	284.8	107.3	313.0	0.9	1.6	0.1	34.9	56.8	84.4	33.6	0.6	1.1
Minimum	685.5	306.8	1764.4	3.6	1.1	0.2	90.7	517.4	1816.1	7.3	0.2	9.0
Maximum	2147.7	877.6	3100.8	7.5	6.7	0.7	251.1	770.6	2204.3	164.1	2.9	14.1
RG-1 (n=33)												
Mean	619.8	612.0	1587.5	12.5	12.3	1.2	53.6	527.9	2265.6	277.3	0.7	12.3
Median	633.4	602.9	1550.2	11.5	4.3	1.1	52.6	506.7	2145.7	234.1	0.7	11.7
Standard Deviation	123.5	207.3	396.4	6.3	30.8	0.7	18.8	132.0	1008.7	215.0	0.4	4.3
Minimum	380.9	259.0	938.2	3.5	1.4	0.2	27.7	309.0	678.5	18.1	0.1	5.6
Maximum	898.9	1081.6	2527.2	25.8	173.6	2.6	120.5	830.7	4108.3	1041.1	1.8	20.8
RG-2 (n=34)												
Mean	573.6	388.7	1289.7	6.1	8.1	0.7	43.3	396.9	1301.1	127.7	0.3	7.6
Median	570.9	372.2	1257.2	4.8	2.7	0.5	36.9	380.0	1225.0	56.3	0.2	7.0
Standard Deviation	170.6	95.0	257.4	4.1	14.2	0.4	17.3	87.3	444.9	174.2	0.3	2.7
Minimum	338.7	249.0	852.3	1.3	0.4	0.1	23.9	266.7	568.9	0.0	0.0	3.7
Maximum	883.8	592.8	1849.8	22.5	60.6	2.0	95.4	621.9	2323.0	764.2	1.8	15.1

271

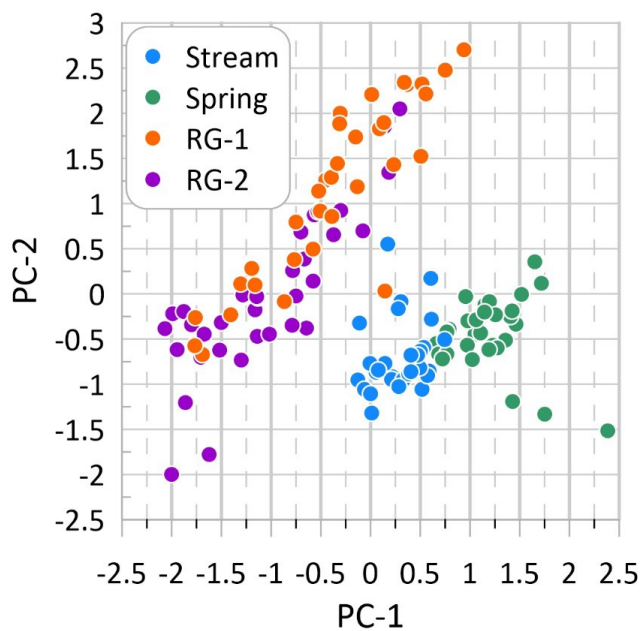
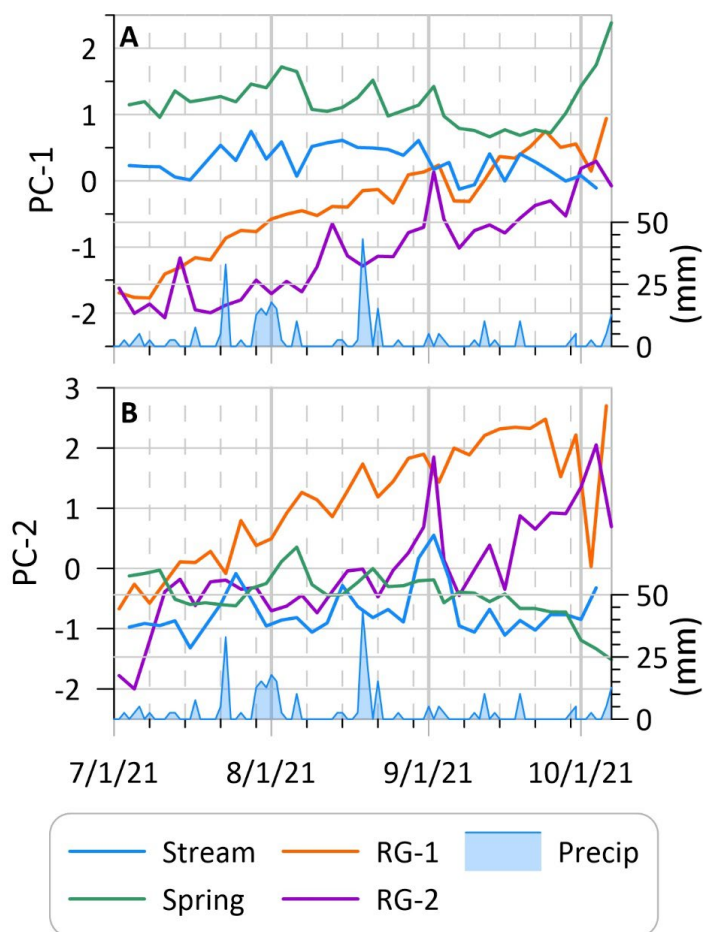


Figure 7: Biplot of the first and second principle components determined for major elements in the water samples. The similarity of the rock glacier water samples is clear, as is their lack of overlap with the Stream and Spring samples.



286

287 **Figure 8:** Time series of the first and second principle components presented in Figure 7. Values tend to be stable
288 through the melt season at the Stream and Spring, but rise notably at both the rock glacier sites.

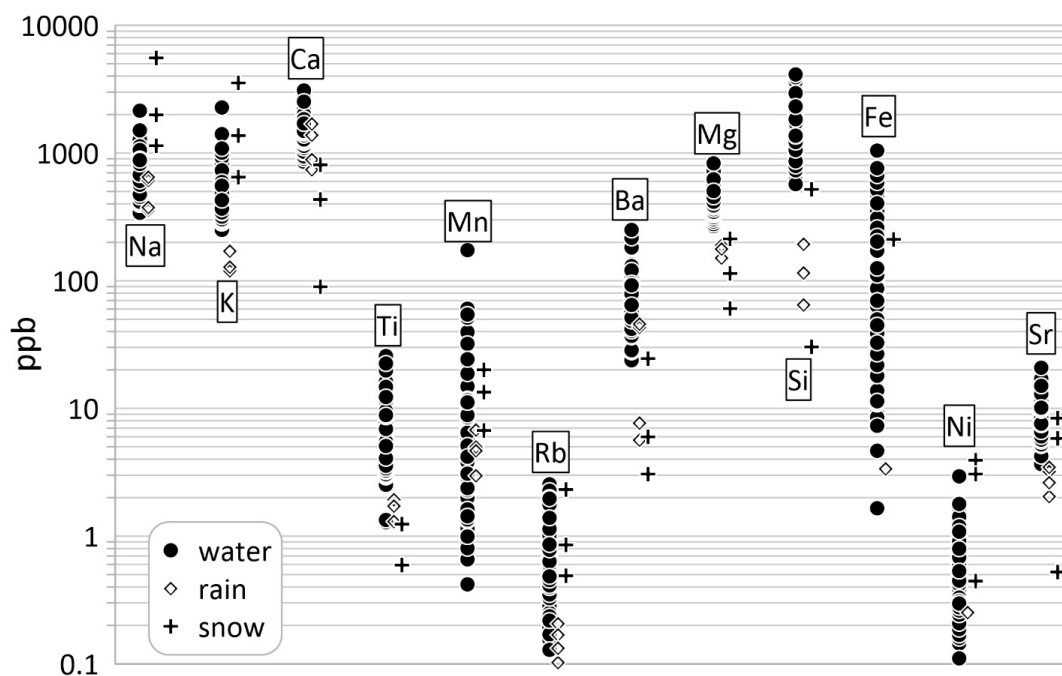
289

290 close for the Stream and Spring. There is a slight tendency for $\delta^{18}\text{O}$ to increase $\sim 0.2\%$ over the course of the
291 summer, which is consistent with evaporation, however this shift is far less than the changes observed in these
292 sequences of samples from start to finish. Thus, the time-series are interpreted without significant concern that
293 values were altered by evaporation.

294 The sampling and analysis strategy in this project was designed to evaluate whether water draining from
295 representative rock glaciers in the Uinta Mountains differs from streamwater and ground water in a manner that is
296 consistent with the presence of melting ice within the rock glacier. The summer of 2021 was a particularly
297 appropriate time to attempt this because the snowpack during the preceding winter was notably below average. On



298 April 1, 2021 the Chepeta SNOTEL (Figure 1) was at 83% of the 1991-2020 median of 380 mm snow water



299

300 **Figure 9:** Abundances of detectable elements in the time series of water samples, along with the rain and snow
301 samples. Note the logarithmic scale on the Y-axis.

302 equivalent (SWE), but by April 13, the average date of the annual peak, SWE was just 52% of average (188 mm).
303 In contrast to other years in which we have conducted fieldwork at the RG-1 and RG-2 sites, the surfaces of the rock
304 glaciers were notably snow free when the samplers were deployed in early July. Inspection of high-resolution
305 satellite imagery confirms that visible snow on the rock glacier surfaces disappeared by the end of June, and that
306 essentially no snow was present anywhere in the West Fork Whiterocks Drainage after the start of July. Therefore,
307 it is unlikely that the water collected at RG-1 and RG-2, particularly late summer and fall, was sourced from melting
308 snow.

309 Analysis of stable isotopes reveals contrast between the water types that can be linked back to their sources
310 and flowpaths. Groundwater from the spring exhibits the most depleted $\delta^{18}\text{O}$, with values similar to snow (Figure
311 6). This correspondence suggests that the groundwater system is primarily recharged by snowmelt. The average
312 annual maximum SWE at the Chepeta SNOTEL station of 380 mm equals half of the mean annual precipitation.
313 The snowmelt pulse in the spring, therefore, is apparently the only precipitation event of the year that can
314 overwhelm the moisture holding capacity of the soil and pass water into the groundwater system. The consistently
315 low $\delta^{18}\text{O}$ values of the water discharging from the spring during the course of the summer, despite numerous
316 rainstorms delivering isotopically less depleted water, emphasizes that the deeper groundwater system is snow-
317 dominated and stable.



318 Samples from RG-1 and RG-2 from the early part of the melt season plot on the GMWL, with low values
319 consistent with a large contribution of snowmelt (Figure 5). Even though visible snow was absent from the rock
320 glacier surfaces at this time, this correspondence indicates that snow was still melting within the interstices between
321 blocks on the rock glacier surface, a situation that was reported by previous studies (Krainer et al., 2007). By the
322 beginning of August, however, isotope values at both rock glacier springs depart from the GMWL and rise to higher
323 values of *d-excess* (Figure 5). This pattern is not seen in the Spring or the Stream time-series, which remain on the
324 GMWL from start to finish. Thus, late summer and fall water discharging from both rock glaciers is distinct from
325 contemporary precipitation and ground water. This pattern is particularly dramatic at RG-1, where all of the August
326 through October samples cluster around a $\delta^{18}\text{O}$ of -13‰ with *d-excess* values as high as 20‰. Previous work on
327 rock glacier hydrology has reported high values of *d-excess* in late-summer rock glacier discharge, and interpreted
328 them as a signal of melting internal rock glacier ice that has undergone numerous freeze/thaw cycles (Steig et al.,
329 1998; Williams et al., 2006).

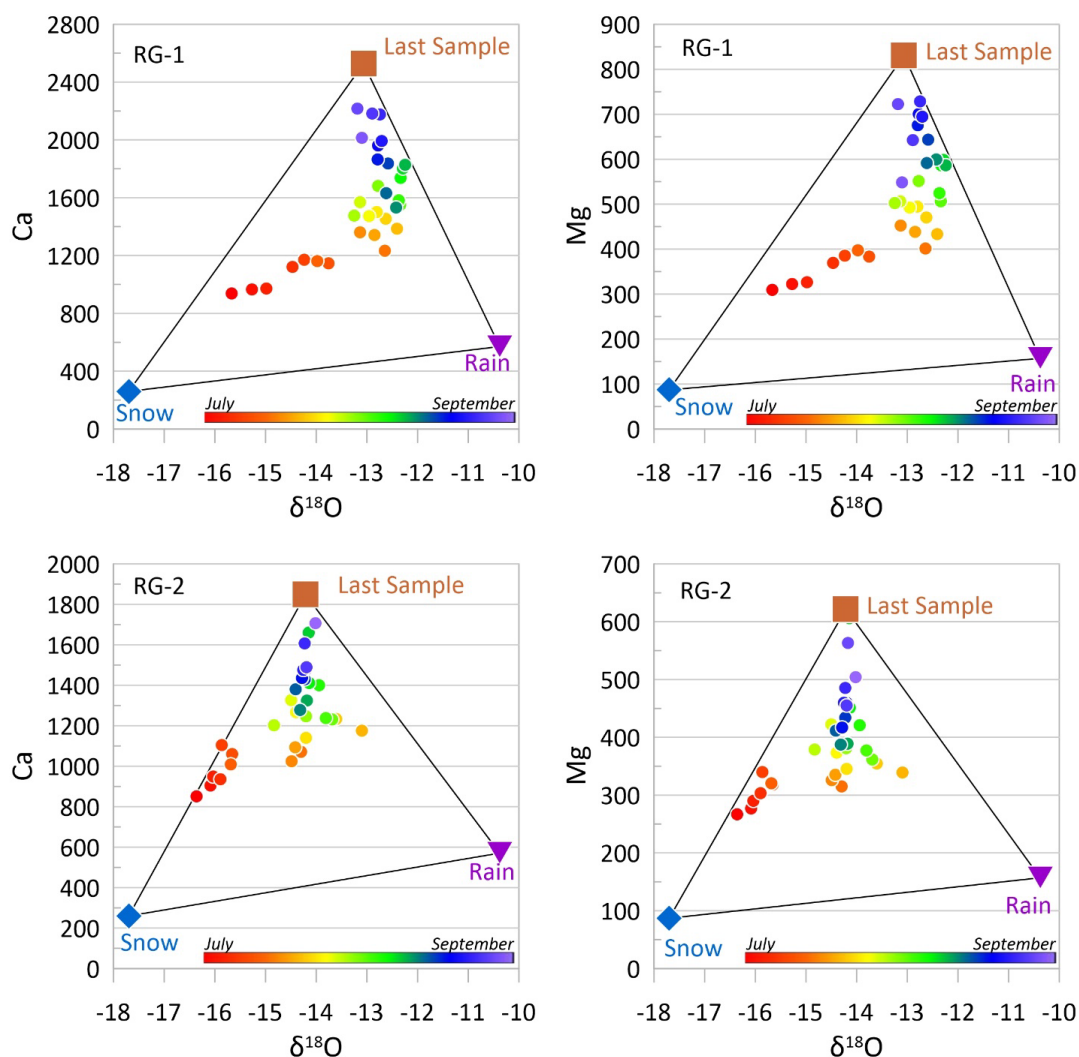
330 The time-series of PC values reinforce the uniqueness of the rock glacier water. Values for the Spring and
331 for the Stream are notably stable through the summer and into the fall (Figure 8). This consistency suggests that
332 these systems are not directly impacted by short-term events like rainstorms, or even changes over seasonal
333 timescales, presumably due to their well-mixed nature and large reservoirs. In contrast, the time series for the two
334 rock glacier springs rise dramatically during the melt season. Values of PC-1 increase starting at the beginning of
335 July in both records; values of PC-2 start rising in July for RG-1 and in mid-August for RG-2. Concentrations for
336 many individual elements increase by a factor of 3 or more from early July until October. This enrichment is
337 consistent with movement of water through the fine matrix of crushed rock material in the rock glacier interior,
338 where fresh mineral grains are available for rapid chemical weathering by cold water charged with carbonic acid
339 (Krainer and Mostler, 2002; Williams et al., 2006). Melting of ice would both liberate meltwater and open
340 flowpaths through this material. The pattern of rising dissolved load through the summer, therefore, provides
341 additional support for the interpretation that the source of the water draining from the rock glaciers shifts after
342 snowmelt is over.

343 The transition in source of the water draining from the rock glaciers is further illustrated by biplots of $\delta^{18}\text{O}$
344 against Ca and Mg content (Figure 10). Values for snow, rain, and the last sample from each rock glacier define a
345 triangle entirely enclosing samples collected from the rock glaciers. Water draining from the rock glaciers in July
346 exhibits a clear snowmelt influence, but this diminishes in August as the water becomes a more even mixture of rain
347 and rock glacier water. Through September into October, this balance shifts away from rain, eventually reaching a
348 minimal rain contribution in the last water discharged before the system froze up for the winter.

349 Williams et al. (2006) proposed a model for changing flowpaths and water sources over the course of the
350 melt season that is relevant for interpreting the results presented here. In early summer, the interior of a rock glacier
351 is frozen and water derived from snowmelt is discharged after draining through the blocky surface layer and running
352 along the top of the frozen core (Krainer and Mostler, 2002). Later in the summer, snowmelt is finished and



353 seasonal ice within the rock glacier begins to melt, opening flowpaths that bring meltwater into contact with fresh



354

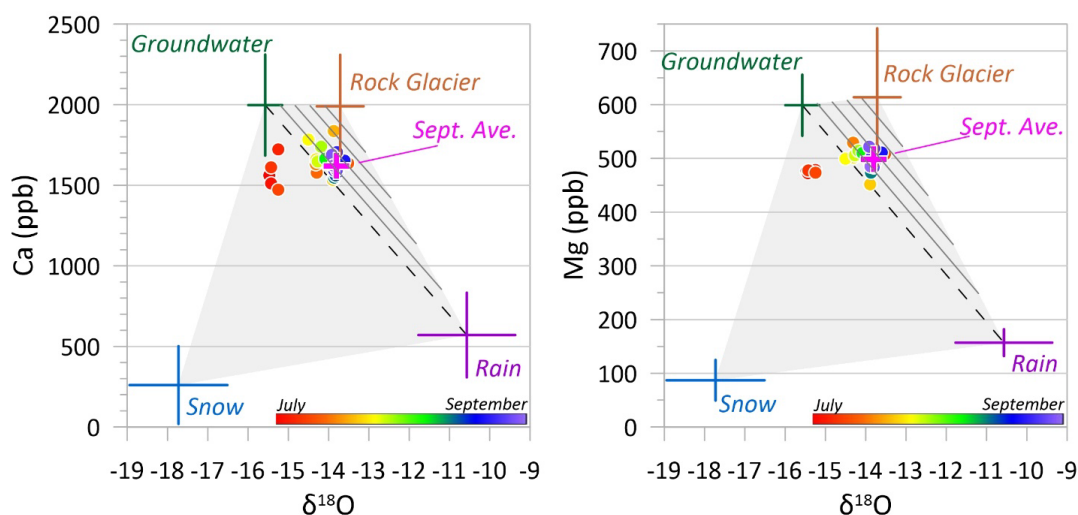
355 **Figure 10:** Biplots of $\delta^{18}\text{O}$ vs. Ca and Mg at RG-1 and RG-2. Circles represent water discharging from the rock
356 glacier springs, with the rainbow pattern progressing from early July (red) through to early October (purple). The
357 last sample collected at each rock glacier is plotted as the brown square, along with average values for snow and
358 rain. Rock glacier water clearly evolves through the season from a composition dominated by snowmelt, to a
359 mixture of rain and internal water, with decreasing rain influence over time.

360 highly weatherable mineral grains. Finally, in late summer and the fall, older perennial ice within the rock glacier
361 begins to melt (Williams et al., 2007), liberating water with high dissolved load and uniquely high values of *d-excess*
362 due reflecting a history of multiple freeze/thaw cycles. The isotopic and hydrochemical results presented here are
363 consistent with this model, supporting the interpretation that water discharging from Uinta rock glaciers in late
364 summer and fall is derived from the melting of perennial internal ice.



365 5.2 Implications for High Mountain Hydrology

366 The rock glaciers studied in this project are but two of eight mapped within the West Fork Whiterocks watershed
367 (Munroe, 2018), which also hosts extensive talus (Munroe and Laabs, 2009) that may contain non-trivial amounts of
368 ice. It is reasonable to predict, therefore, that water derived from rock glaciers may comprise an important amount
369 of the overall streamflow in the latter part of the summer and fall. Figure 11 presents biplots of $\delta^{18}\text{O}$ vs. Ca and Mg
370 content, two elements that are notably elevated in the late summer rock glacier water in the Uintas and elsewhere
371 (Williams et al., 2006).



372

373 **Figure 11:** Biplots of $\delta^{18}\text{O}$ vs. Ca and Mg used to determine the contribution of rock glacier discharge to
374 streamflow. Water in the stream is plotted with a rainbow pattern progressing from July (red) through to early
375 October (purple). Crosses represent the end members of snow, rain, groundwater, and rock glacier water. July
376 streamwater samples contain a mixture of snowmelt and groundwater, but in August and September, snowmelt is
377 now longer detectable (samples to right of dashed line). Streamwater samples at this time contain non-trivial
378 amounts of water derived from rock glaciers, with an average of 25% in September (pink cross). Diagonal black
379 lines denote the abundance of rock glacier water in increments of 20% for emphasis.

380 After Krainer and Mostler (2002), four end member sources of water to the stream are: groundwater, snow, rain, and
381 rock glaciers. The groundwater end member is constrained for the 2021 melt season by the 33 samples from the
382 non-rock glacier spring. The snow end member is less well constrained, however the two grab samples collected in
383 July from RG-1 and RG-2 have isotope values consistent with snow previously analyzed from the Uintas (Munroe,
384 2021) and with values predicted by the OPIC. Thus these samples are considered a valid representation of the snow
385 lingering in the Whiterocks River watershed in the summer of 2021. Five samples (two from RG-1 and three from
386 RG-2) collected from the rock glacier springs in October immediately before freeze up represent the rock glacier
387 meltwater end member. Finally, two precipitation samples from RG-2 and two from the spring site are available to



388 represent rain. However, the concentration of Ca in the Spring sampler is ~3x higher than at RG-2, despite the
389 distance of only 3 km between the two sites. The precipitation sampler at the Spring site is located close to a dirt
390 road though, raising the possibility that dust produced by vehicle traffic raised the Ca content of the water collected
391 at this site. Support for this interpretation is provided by 7 years of unpublished precipitation chemistry (n=79
392 samples) collected by the USDA-Ashley National Forest in the Uintas. Concentrations of Ca in this dataset average
393 645 ppb, similar to the value of 570 ppb in the rain from the precipitation sampler at RG-2 and notably less than
394 mean of 1535 ppb at the roadside Spring site. Thus, the precipitation samples from RG-2 alone are taken to
395 represent the rain end member in the stream system for the melt season of 2021.

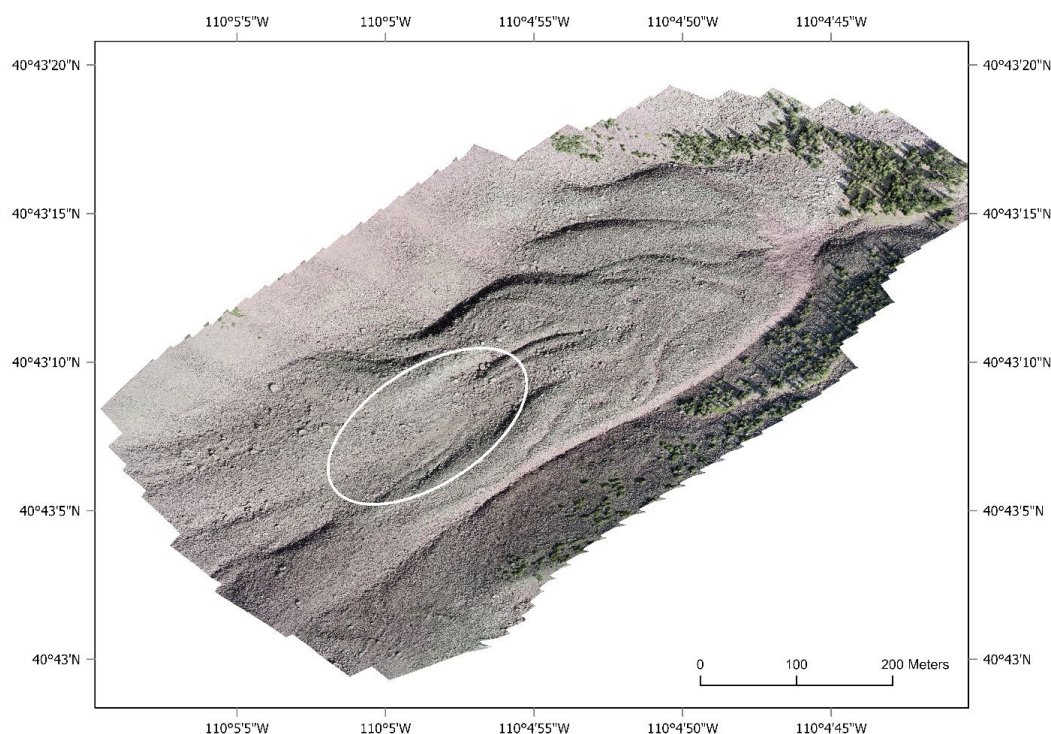
396 With this approach, the four end members define a polygon entirely surrounding the streamwater samples
397 (Figure 11). As in the time-series from the individual rock glaciers (Figure 5), a clear transition is notable. July
398 streamwater samples exhibit $\delta^{18}\text{O}$ values similar to snowmelt and groundwater, whereas late summer and fall
399 samples plot entirely within a triangle bounded by the groundwater, rock glacier, and rain. Within this triangle,
400 although the proportions vary somewhat between samples, individual streamwater samples from August and
401 September can be visually separated as a mixture of ~20-30% rain, ~25 to 75% groundwater, and up to 50% rock
402 glacier water. The overall mean of September streamwater samples can be defined as ~25% rain, ~50%
403 groundwater, and ~25% rock glacier water. Water with a signature similar to that of springs discharging directly
404 from rock glacier termini, therefore, generally makes up a quarter of all the water flowing in the master stream of
405 this drainage after snowmelt has ended.

406 With such a significant contribution of rock glacier meltwater to streamflow in this system, it is worth
407 considering whether rock glacier ice is melting at an unsustainable rate. This possibility is hard to evaluate directly,
408 given that mass balance techniques for ice glacier systems are difficult to apply to rock glaciers (Østrem and
409 Brugman, 1966). Nonetheless, it is notable that a depression consistent with subsidence accompanying the melt-out
410 of an ice core is present in the upper part of RG-2 (Figure 12). A high-resolution topographic model constructed for
411 this rock glacier using structure-from-motion applied to images collected with an uncrewed aerial vehicle (UAV)
412 reveals that this depression has an area of 19,350 m² and a volume of 106,500 m³ (mean depth of 5.5 m). If this
413 depression formed due to the loss of ice, this volume corresponds to ~10⁸ L of water. At rates of 10² to 10³ L/min
414 estimated for the modern flow, that equates to 70 to 700 days. Thus, ice within this rock glacier may have begun
415 melting unsustainably in the past few decades in response to rising summer temperatures noted in Uinta climate
416 records (Brencher et al., 2021). Future InSAR monitoring may help constrain subsidence on this and other rock
417 glaciers, yielding additional information about the response of these features to contemporary climate warming and
418 likely changes in their future contributions to high-elevation hydrology.

419

420 **6 Conclusion**

421 Time series of samples collected during the summer of 2021 reveal that water draining from rock glaciers in the
422 Uinta Mountains of Utah (USA) has a composition distinct from groundwater and from water in the master stream



423
424 **Figure 12:** True-color hillshaded photomosaic of RG-2 produced by structure from motion (SfM) applied to a set of
425 243 images collected at an altitude of 120 m above the ground. The white oval highlights the prominent depression
426 near the head of the rock glacier, which may reflect subsidence due to ice meltout.

427

428 of a representative 5000-ha drainage. Rock glacier water resembles snowmelt in the early summer, but transitions to
429 higher values of *d-excess* and greatly elevated Ca and Mg content as the melt season progresses. This pattern is
430 consistent with models describing a change in water source from snowmelt, to melting of seasonal ice, to melting of
431 deeper perennial ice in the rock glacier interior in late summer and fall. Water derived from this internal ice appears
432 to have been the source of ~25% of the streamflow in this study area during September of 2021. This result
433 emphasizes the significant role that rock glaciers can play in the hydrology of high-elevation watersheds,
434 particularly in melt seasons following a winter with below average snowpack.

435

436

437



438 **Author Contributions**

439 JM designed the project, conducted the fieldwork and laboratory analyses, interpreted the results, and drafted the
440 figures. JS prepared the manuscript with contributions from AH.

441

442 **Competing Interests:** The authors declare that they have no conflict of interest.

443

444 **Acknowledgements**

445 This work was supported by NSF HS-1935200 to PIs Munroe and Handwerger, and NSF MRI-1918436 to Munroe.
446 The authors thank Q. Brencher, C. Klutmeier, S. Lusk, E. Norris, A. Santis, and A. Takoudes for their assistance in
447 the field, and E. McMahon for help preparing the water samplers.



448 **References Cited**

- 449 Adler, C., Huggel, C., Orlove, B., and Nolin, A., 2019, Climate change in the mountain cryosphere: impacts and
450 responses: *Regional Environmental Change*, v. 19, p. 1225–1228.
- 451 Albrich, K., Rammer, W., and Seidl, R., 2020, Climate change causes critical transitions and irreversible alterations
452 of mountain forests: *Global change biology*, v. 26, p. 4013–4027.
- 453 Alexander, J.M., Chalmandrier, L., Lenoir, J., Burgess, T.I., Essl, F., Haider, S., Kueffer, C., McDougall, K.,
454 Milbau, A., and Nuñez, M.A., 2018, Lags in the response of mountain plant communities to climate
455 change: *Global change biology*, v. 24, p. 563–579.
- 456 Atwood, W.W., 1909, *Glaciation of the Uinta and Wasatch mountains*: US Government Printing Office, v. 61.
- 457 Azócar, G.F., and Brenning, A., 2010, Hydrological and geomorphological significance of rock glaciers in the dry
458 Andes, Chile (27–33 S): *Permafrost and Periglacial Processes*, v. 21, p. 42–53.
- 459 Beniston, M., Farinotti, D., Stoffel, M., Andreassen, L.M., Coppola, E., Eckert, N., Fantini, A., Giacona, F., Hauck,
460 C., and Huss, M., 2018, The European mountain cryosphere: a review of its current state, trends, and future
461 challenges: *The Cryosphere*, v. 12, p. 759–794.
- 462 Biskaborn, B.K. et al., 2019, Permafrost is warming at a global scale: *Nature Communications*, v. 10, p. 264,
463 doi:10.1038/s41467-018-08240-4.
- 464 Bonfils, C., Santer, B.D., Pierce, D.W., Hidalgo, H.G., Bala, G., Das, T., Barnett, T.P., Cayan, D.R., Doutriaux, C.,
465 and Wood, A.W., 2008, Detection and attribution of temperature changes in the mountainous western
466 United States: *Journal of Climate*, v. 21, p. 6404–6424.
- 467 Bowen, G.J., and Revenaugh, J., 2003, Interpolating the isotopic composition of modern meteoric precipitation:
468 *Water Resources Research*, v. 39, <http://onlinelibrary.wiley.com/doi/10.1029/2003WR002086/full>
469 (accessed January 2017).
- 470 Bowen, G.J., and Wilkinson, B., 2002, Spatial distribution of $\delta^{18}\text{O}$ in meteoric precipitation: *Geology*, v. 30, p.
471 315–318.
- 472 Brencher, G., Handwerger, A.L., and Munroe, J.S., 2021, InSAR-based characterization of rock glacier movement
473 in the Uinta Mountains, Utah, USA: *The Cryosphere*, v. 15, p. 4823–4844.
- 474 Brighenti, S., Hotaling, S., Finn, D.S., Fountain, A.G., Hayashi, M., Herbst, D., Saros, J.E., Tronstad, L.M., and
475 Millar, C.I., 2021, Rock glaciers and related cold rocky landforms: Overlooked climate refugia for
476 mountain biodiversity: *Global Change Biology*, v. 27, p. 1504–1517.
- 477 Buchli, T., Kos, A., Limpach, P., Merz, K., Zhou, X., and Springman, S.M., 2018, Kinematic investigations on the
478 Furggwanghom rock glacier, Switzerland: *Permafrost and Periglacial Processes*, v. 29, p. 3–20.
- 479 Catalan, J., Ninot, J.M., and Aniz, M.M., 2017, *High mountain conservation in a changing world*: Springer Nature.
- 480 Chakraborty, A., 2021, Mountains as vulnerable places: a global synthesis of changing mountain systems in the
481 Anthropocene: *GeoJournal*, v. 86, p. 585–604.
- 482 Craig, H., 1961, Isotopic variations in meteoric waters: *Science*, v. 133, p. 1702–1703.
- 483 Dansgaard, W., 1964, Stable isotopes in precipitation: *Tellus*, v. 16, p. 436–468.



- 484 Dehler, C.M., Porter, S.M., De Grey, L.D., Sprinkel, D.A., and Brehm, A., 2007, The Neoproterozoic Uinta
485 Mountain Group revisited; a synthesis of recent work on the Red Pine Shale and related undivided clastic
486 strata, northeastern Utah, U. S. A (P. K. Link & R. S. Lewis, Eds.): Special Publication - Society for
487 Sedimentary Geology, v. 86, p. 151–166.
- 488 Egan, P.A., and Price, M.F., 2017, Mountain ecosystem services and climate change: A global overview of potential
489 threats and strategies for adaptation:
- 490 von Freyberg, J., Knapp, J.L.A., Rücker, A., Studer, B., and Kirchner, J.W., 2020, Technical note: Evaluation of a
491 low-cost evaporation protection method for portable water samplers: Hydrology and Earth System
492 Sciences, v. 24, p. 5821–5834, doi:10.5194/hess-24-5821-2020.
- 493 Geiger, S.T., Daniels, J.M., Miller, S.N., and Nicholas, J.W., 2014, Influence of rock glaciers on stream hydrology
494 in the La Sal Mountains, Utah: Arctic, Antarctic, and Alpine Research, v. 46, p. 645–658.
- 495 Giardino, J.R., Shroder, J.F., and Vitek, J.D., 1987, Rock glaciers: Allen & Unwin London.
- 496 Giardino, J.R., and Vitek, J.D., 1988, The significance of rock glaciers in the glacial-periglacial landscape
497 continuum: Journal of Quaternary Science, v. 3, p. 97–103, doi:10.1002/jqs.3390030111.
- 498 Gröning, M., Lutz, H.O., Roller-Lutz, Z., Kralik, M., Gourcy, L., and Pölsenstein, L., 2012, A simple rain collector
499 preventing water re-evaporation dedicated for $\delta^{18}\text{O}$ and $\delta^2\text{H}$ analysis of cumulative precipitation samples:
500 Journal of Hydrology, v. 448, p. 195–200.
- 501 Halla, C., Blöthe, J.H., Tapia Baldis, C., Trombotto Liaudat, D., Hilbich, C., Hauck, C., and Schrott, L., 2021, Ice
502 content and interannual water storage changes of an active rock glacier in the dry Andes of Argentina: The
503 Cryosphere, v. 15, p. 1187–1213.
- 504 Hansen, W.R., 1986, Neogene tectonics and geomorphology of the eastern Uinta Mountains in Utah, Colorado, and
505 Wyoming: United States Geological Survey, Professional Paper, v. 75.
- 506 Harrington, J.S., Mozil, A., Hayashi, M., and Bentley, L.R., 2018, Groundwater flow and storage processes in an
507 inactive rock glacier: Hydrological Processes, v. 32, p. 3070–3088.
- 508 Huss, M., Bookhagen, B., Huggel, C., Jacobsen, D., Bradley, R.S., Clague, J.J., Vuille, M., Buytaert, W., Cayan,
509 D.R., and Greenwood, G., 2017, Toward mountains without permanent snow and ice: Earth's Future, v. 5,
510 p. 418–435.
- 511 Janke, J.R., Ng, S., and Bellisario, A., 2017, An inventory and estimate of water stored in firn fields, glaciers,
512 debris-covered glaciers, and rock glaciers in the Aconcagua River Basin, Chile: Geomorphology, v. 296, p.
513 142–152.
- 514 Johnson, G., Chang, H., and Fountain, A., 2021, Active rock glaciers of the contiguous United States: geographic
515 information system inventory and spatial distribution patterns: Earth System Science Data, v. 13, p. 3979–
516 3994, doi:10.5194/essd-13-3979-2021.
- 517 Jones, D.B., Harrison, S., Anderson, K., Selley, H.L., Wood, J.L., and Betts, R.A., 2018, The distribution and
518 hydrological significance of rock glaciers in the Nepalese Himalaya: Global and Planetary Change, v. 160,
519 p. 123–142.
- 520 Jones, D.B., Harrison, S., Anderson, K., and Whalley, W.B., 2019, Rock glaciers and mountain hydrology: A
521 review: Earth-Science Reviews, v. 193, p. 66–90, doi:10.1016/j.earscirev.2019.04.001.



- 522 Kenner, R., Phillips, M., Limpach, P., Beutel, J., and Hiller, M., 2018, Monitoring mass movements using
523 georeferenced time-lapse photography: Ritigraben rock glacier, western Swiss Alps: *Cold Regions Science*
524 and *Technology*, v. 145, p. 127–134.
- 525 Konrad, S.K., Humphrey, N.F., Steig, E.J., Clark, D.H., Potter, N., and Pfeffer, W.T., 1999, Rock glacier dynamics
526 and paleoclimatic implications: *Geology*, v. 27, p. 1131–1134.
- 527 Krainer, K. et al., 2015, A 10,300-year-old permafrost core from the active rock glacier Lazaun, southern Ötztal
528 Alps (South Tyrol, northern Italy): *Quaternary Research*, v. 83, p. 324–335,
529 doi:10.1016/j.yqres.2014.12.005.
- 530 Krainer, K., and Mostler, W., 2002, Hydrology of active rock glaciers: examples from the Austrian Alps: *Arctic,*
531 *Antarctic, and Alpine Research*, p. 142–149.
- 532 Krainer, K., Mostler, W., and Spötl, C., 2007, DISCHARGE FROM ACTIVE ROCK GLACIERS, AUSTRIAN
533 ALPS: A STABLE ISOTOPE APPROACH.: *Austrian Journal of Earth Sciences*, v. 100.
- 534 Lehmann, B., Anderson, R.S., Bodin, X., Cusicanqui, D., Valla, P.G., and Carcaillet, J., 2022, Alpine rock glacier
535 activity over Holocene to modern timescales (western French Alps): *Earth Surface Dynamics Discussions*,
536 p. 1–40.
- 537 McDowell, G., Huggel, C., Frey, H., Wang, F.M., Cramer, K., and Ricciardi, V., 2019, Adaptation action and
538 research in glaciated mountain systems: Are they enough to meet the challenge of climate change? *Global*
539 *Environmental Change*, v. 54, p. 19–30.
- 540 Millar, C.I., and Westfall, R.D., 2010, Distribution and climatic relationships of the American pika (*Ochotona*
541 *princeps*) in the Sierra Nevada and western Great Basin, USA; periglacial landforms as refugia in warming
542 climates: *Arctic, Antarctic, and Alpine Research*, v. 42, p. 76–88.
- 543 Millar, C.I., Westfall, R.D., Evenden, A., Holmquist, J.G., Schmidt-Gengenbach, J., Franklin, R.S., Nachlinger, J.,
544 and Delany, D.L., 2015, Potential climatic refugia in semi-arid, temperate mountains: Plant and arthropod
545 assemblages associated with rock glaciers, talus slopes, and their forefield wetlands, Sierra Nevada,
546 California, USA: *Quaternary International*, v. 387, p. 106–121, doi:10.1016/j.quaint.2013.11.003.
- 547 Minder, J.R., Letcher, T.W., and Liu, C., 2018, The character and causes of elevation-dependent warming in high-
548 resolution simulations of Rocky Mountain climate change: *Journal of Climate*, v. 31, p. 2093–2113.
- 549 Munroe, J.S., 2018, Distribution, evidence for internal ice, and possible hydrologic significance of rock glaciers in
550 the Uinta Mountains, Utah, USA: *Quaternary Research*, v. 90, p. 1–16.
- 551 Munroe, J.S., 2021, First Investigation of Perennial Ice in Winter Wonderland Cave, Uinta Mountains, Utah, USA:
552 *The Cryosphere*, v. 15, p. 863–881, doi:doi.org/10.5194/tc-15-863-2021.
- 553 Munroe, J.S., 2006, Investigating the spatial distribution of summit flats in the Uinta Mountains of northeastern
554 Utah, USA: *Geomorphology*, v. 75, p. 437–449.
- 555 Munroe, J.S., and Laabs, B.J.C., 2009, Glacial Geologic Map of the Uinta Mountains Area, Utah and Wyoming.:
556 *Utah Geological Survey Miscellaneous Publication 09-4DM*, scale Map.
- 557 Østrem, G., and Brugman, M., 1966, Glacier mass balance measurements: Department of Mines and Technical
558 Surveys, Glaciology Section.
- 559 Palomo, I., 2017, Climate change impacts on ecosystem services in high mountain areas: a literature review:
560 *Mountain Research and Development*, v. 37, p. 179–187.



- 561 Petersen, E.I., Levy, J.S., Holt, J.W., and Stuurman, C.M., 2020, New insights into ice accumulation at Galena
562 Creek Rock Glacier from radar imaging of its internal structure: *Journal of Glaciology*, v. 66, p. 1–10.
- 563 Rangecroft, S., Harrison, S., and Anderson, K., 2015, Rock Glaciers as Water Stores in the Bolivian Andes: An
564 Assessment of Their Hydrological Importance: *Arctic, Antarctic, and Alpine Research*, v. 47, p. 89–98,
565 doi:10.1657/AAAR0014-029.
- 566 Rödder, D., Schmitt, T., Gros, P., Ulrich, W., and Habel, J.C., 2021, Climate change drives mountain butterflies
567 towards the summits: *Scientific reports*, v. 11, p. 1–12.
- 568 Rowan, A.V., Quincey, D.J., Gibson, M.J., Glasser, N.F., Westoby, M.J., Irvine-Fynn, T.D., Porter, P.R., and
569 Hambrey, M.J., 2018, The sustainability of water resources in High Mountain Asia in the context of recent
570 and future glacier change: *Geological Society, London, Special Publications*, v. 462, p. 189–204.
- 571 Sakai, A., and Fujita, K., 2017, Contrasting glacier responses to recent climate change in high-mountain Asia:
572 *Scientific reports*, v. 7, p. 1–8.
- 573 Sears, J., Graff, P., and Holden, G., 1982, Tectonic evolution of lower Proterozoic rocks, Uinta Mountains, Utah and
574 Colorado: *Geological Society of America Bulletin*, v. 93, p. 990–997.
- 575 Sommer, C., Malz, P., Seehaus, T.C., Lippl, S., Zemp, M., and Braun, M.H., 2020, Rapid glacier retreat and
576 downwasting throughout the European Alps in the early 21st century: *Nature Communications*, v. 11, p. 1–
577 10.
- 578 Steig, E.J., Fitzpatrick, J.J., Potter, N., and Clark, D.H., 1998, The geochemical record in rock glaciers: *Geografiska
579 Annaler: Series A, Physical Geography*, v. 80, p. 277–286.
- 580 Stoffel, M., and Corona, C., 2018, Future winters glimpsed in the Alps: *Nature Geoscience*, v. 11, p. 458–460.
- 581 Strozzi, T., Caduff, R., Jones, N., Barboux, C., Delaloye, R., Bodin, X., Käab, A., Mätzler, E., and Schrott, L., 2020,
582 Monitoring rock glacier kinematics with satellite synthetic aperture radar: *Remote Sensing*, v. 12, p. 559.
- 583 Thaler, T., Zischg, A., Keiler, M., and Fuchs, S., 2018, Allocation of risk and benefits—distributional justices in
584 mountain hazard management: *Regional environmental change*, v. 18, p. 353–365.
- 585 Wagner, T., Brodacz, A., Krainer, K., and Winkler, G., 2020, Active rock glaciers as shallow groundwater
586 reservoirs, Austrian Alps: *Grundwasser*, v. 25, p. 215–230.
- 587 Wagner, T., Kainz, S., Helfricht, K., Fischer, A., Avian, M., Krainer, K., and Winkler, G., 2021, Assessment of
588 liquid and solid water storage in rock glaciers versus glacier ice in the Austrian Alps: *Science of the Total
589 Environment*, v. 800, p. 149593.
- 590 Wahrhaftig, C., and Cox, A., 1959, Rock glaciers in the Alaska Range: *Geological Society of America Bulletin*, v.
591 70, p. 383–436.
- 592 Williams, M.W., Knauf, M., Caine, N., Liu, F., and Verplanck, P.L., 2006, Geochemistry and source waters of rock
593 glacier outflow, Colorado Front Range: *Permafrost and Periglacial Processes*, v. 17, p. 13–33,
594 doi:10.1002/ppp.535.
- 595 Williams, M.W., Knauf, M., Cory, R., Caine, N., and Liu, F., 2007, Nitrate content and potential microbial signature
596 of rock glacier outflow, Colorado Front Range: *Earth Surface Processes and Landforms*, v. 32, p. 1032–
597 1047, doi:10.1002/esp.1455.



598 Xenarios, S., Gafurov, A., Schmidt-Vogt, D., Sehring, J., Manandhar, S., Hergarten, C., Shigaeva, J., and Foggin,
599 M., 2019, Climate change and adaptation of mountain societies in Central Asia: uncertainties, knowledge
600 gaps, and data constraints: Regional Environmental Change, v. 19, p. 1339–1352.

601